Ezetimibe anticancer activity via the p53/Mdm2 pathway: Implications for RBBP6

Charmy Twala
University of South Africa
Bonnie Russell
University of South Africa
Sibusiso Malindisa
University of South Africa
Chamone Munnik
University of South Africa
Selisha Sooklal
University of South Africa
Monde Ntwasa
ntwasmm@unisa.ac.za

University of South Africa

Article

Keywords: RBBP6, p53, Mdm2, drug design, drug development, drug repurposing, ezetimibe, cancer

Posted Date: March 14th, 2024

DOI: https://doi.org/10.21203/rs.3.rs-3957997/v1

Additional Declarations: No competing interests reported.

Abstract

Ezetimibe is used to treat cardiovascular disease as it blocks the sterol transporter Niemann-Pick C1-Like 1 (NPC1CL1) protein. However, recent evidence indicates that ezetimibe inhibits several cancers, indirectly by reducing circulating cholesterol or via specific signalling pathways. Our *in-silico* studies indicate that ezetimibe binds to the Tp53 binding domain in Mdm2, forming a more thermodynamically stable complex than nutlin3a. Moreover, we show that Tp53 functions in complex with the Retinoblastoma Binding Protein 6 (RBBP6), another negative regulator of p53, and Mdm2. RBBP6 is dysregulated in many cancers, and various studies and may be a prognostic biomarker for certain cancers. We show that ezetimibe inhibits the growth of several cancer cell lines at concentrations that are not toxic to a normal cell line. Thus ezetimibe is probably active against cancers that overexpress Mdm2. Moreover, inhibitors of RBBP6 may be combined with ezetimibe for effective anticancer activity. Due to poor oral bioavailability ezetimibe must be administered parenterally for cancer treatment.

Introduction

Ezetimibe is a United States Food and Drug Administration (FDA) approved drug that blocks cholesterol uptake in the intestines, thereby reducing its concentration in the systemic circulation. It is thus used to treat hypercholesterolemia. Orally administered Ezetimibe is rapidly glucuronidated and recycled by the enterohepatic circulation to its target. It is reported that this glucuronide metabolite is at least as potent as the parent drug in inhibiting cholesterol uptake. This is based on experiments using the initial drug lead, SCH48461, which inhibits cholesterol absorption by 70%, whereas the metabolite inhibited absorption by more than 95%. Furthermore, the metabolite was retained on the intestinal wall, and the bulk of it was not systemically available.

The known target of Ezetimibe is the *Niemann–Pick C1-Like 1* (NPC1L1) found in jejunal enterocytes. Up to 80% of Ezetimibe is rapidly metabolized to its pharmacologically active glucuronide metabolite (EZE-GLUC), by uridine 5-diphosphate (UDP)-glucuronosyl-transferase (UGT) 1A1, 1A3, and 2B15, in the intestine. The remaining parent drug and the glucuronidated metabolite are then excreted into the bile via the portal vein and delivered back into the intestinal site of action, thereby increasing the drug's half-life. Cholesterol absorption studies indicated that the glucuronide appeared more potent than Ezetimibe itself because glucuronidated Ezetimibe localizes more avidly to the intestine. Ezetimibe and/or the glucuronide metabolite are excreted in the faeces (90%) and urine (10%).

The Niemann-Pick C1-Like 1 receptor was identified as a target for Ezetimibe through a systematic search of transcriptomics databases. This discovery was supported by showing that NPC1CL1$^{-/-}$ mice were substantially defective in cholesterol absorption and were resistant to Ezetimibe [1]. Subsequently, a binding assay showed the direct association between Ezetimibe and NPC1CL, by confirming that glucuronidated Ezetimibe binds to the receptor [2].

Experimental evidence has recently supported Ezetimibe as a potential anticancer drug[3]. Some evidence is indirect and based on the function of NPC1L1 as a receptor that mediates cholesterol uptake in the small intestine. For example, NPC1L1$^{-/-}$ mice were found to develop fewer tumours when compared with wild-type mice after the induction of colitis-associated colorectal tumours [4]. In Pancreatic Ductal Adenocarcinoma expressing NPC1CL1, Ezetimibe was toxic and had no effect on fibroblasts [5]. Furthermore, PDAC cells where NPC1L1 was knocked down by siRNA, were resistant to high Ezetimibe concentrations. In another study, Ezetimibe inhibited prostate tumor growth by reducing serum cholesterol, thereby inhibiting angiogenesis [6]. Recent studies show that ezetimibe promotes mitochondrial dysfunction, cell death and cell cyle arrest. In a colorectal cancer cell line ezetimibe induced autophage-associated apoptosis and was associated with the mTOR signalling pathway [7]. In another study, ezetimibe was proposed as a possible treatnebnt for triple negative breast cancer as it blocked the cell cycle in the G1 phase and actvated the PDGFRβ/AKT pathway [8].

The tumour protein p53 (p53) affects several necessary biological processes that are crucial for carcinogenesis, including the cell cycle, apoptosis, DNA repair, angiogenesis, glucose metabolism, and innate immunity [9 10]. A previous study showed that ezetimibe binds snuggly into the p53-binding domain of the Mouse Double Minute (Mdm2) protein [11]. p53 is a transcription factor that functions in an autoregulatory feedback loop with ubiquitin-ligase activity. Thus, as a transcription factor, p53 activates the expression of the gene. On the other hand, Mdm2 regulates p53 by controlling its transport out of the nucleus, making it unavailable to gene targets, inhibiting its transcription function, or promoting its degradation by proteasome using its Ubiquitin-ligase activity. It has been shown in previous studies that the Retinoblastoma Binding Protein 6 (RBBP6) has a similar phenotype with Mdm2 when deleted in mice. Both *mdm2*$^{-/-}$ and *rbbp6* $^{-/-}$ embryos die, a phenotype that a deletion of the p53 gene can rescue. RBBP6 is the p53-associated cellular protein testes derived (PACT) in mice. However, the *rbbp6*$^{-/-}$ phenotype is more severe when compared to the *mdm2*$^{-/-}$, indicating that RBBP6 also functions in pathways independent of Mdm2 [12]. Moreover, RBBP6 is reported to be a prognostic marker and an inducer of cancers such as colorectal and non-small lung cancer [13,14]. Taken together, these findings constitute strong evidence about the druggability of the p53/RBBP6/Mdm2 complex.

Mdm2 has a hydrophobic binding pocket to which p53 binds through a peptide in its transactivation domain[15] (J. Chen et al., 1993; SM Picksley et al., 1994). This pocket is, therefore, a key target for drugs that inhibit the p53-Mdm2 interaction. Indeed, several small molecular drug design studies formulated molecules that can competitively target the Mdm2 p53-binding domain disrupting the formation of Mdm2-p53 complexes and, thus, reactivate p53 levels in cancer cells to promote p53-dependent cell death [16]. In the current study, we provide data reinforcing that RBBP6 may be a scaffold protein that forms a complex with Mdm2 and p53. This suggests that combined targeting of Mdm2 and RBBP6 would produce a good treatment for cancers that overexpress these molecules.

Materials and Methods

Cell lines and cell culture.

The human malignant melanoma cells (A375), pancreatic cancer cells (PANC1), adenocarcinoma human alveolar basal epithelial cell line (A549), human breast cancer cell line (MCF7), human colorectal carcinoma cell line (HT-29) and human embryonic kidney cells (HEK293) were cultured in media containing 89% DMEM (Lonza Bioscience, USA), 10% Foetal Bovine Serum (FBS) (Biowest, USA) and 1% penicillin-streptomycin (Biowest, USA). Once confluent, the cells were washed with 1X phosphate buffered saline (PBS) (Thermo Fisher Scientific, USA) three times and detached from T75 flasks by incubating cells with 2 mL Trypsin-EDTA (Thermo Fisher Scientific, USA) for 5–10 minutes at 37°C. 2 mL DMEM (Lonza Bioscience, USA) was added to the cells to stop the reaction of trypsin-EDTA.

The A549, MCF7 and HEK293 cell lines were obtained from Dr Jitcy Joseph from the National Institute of Occupational Health (NIOH). PANC-1 cells were donated by Dr Ekene Nweke from the University of the Witwatersrand (Wits). A375 and HT-29 cells were purchased from cellonex.

Drugs.

Ezetimibe (SML1629 Sigma-Aldrich)- ≥98% (HPLC). Drug was dissolved in (99.9%) technical grade ethanol (V0T0041, Sigma Aldrich).

Molecular docking studies.

Protein retrieval and preparation.

The MDM2 p53 binding domain crystal structure was retrieved from the protein databank (https://www.rcsb.org/) with Pdb_Id: 1YCR. This protein domain was used as a receptor and prepared to a suitable state for computational calculations using the protein preparation wizard from the Schrödinger suite. During this process missing disulfide bonds, hydrogen atoms, side chains and loops were added using Prime. Water molecules beyond 3Å of the het groups were removed and the hydrogen bonds optimised to avoid steric clashes. The structure was further refined through restrained minimization to an RMSD of 0.3Å.

Ligand database preparation.

The ligand database – Zinc drug database (Zdd) was downloaded from the ZINC12 library (https://zinc12.docking.org/browse/subsets/special) in canonical SMILES format. This database contains 2924 FDA approved compounds which were all prepared to the lowest energy possible 3d configuration by varying tautomeric and ionisation states at a targeted pH range of 7 +/- 2 using Epik. This further generated multiple stereoisomers at a scale of up to 32 compounds per ligand of the original data set. These computations were executed using the OPLS4 force field. Additionally, the Nutlin3A drug was downloaded from the PubChem (https://pubchem.ncbi.nlm.nih.gov/) database and prepared to a suitable 3d configuration state prior docking studies. All computations were done using the ligand preparation wizard in Schrödinger-Maestro v2021-2.

Search space mapping and Grid generation

The docking search space grids were computed using the grid generation panel in Maestro from the Schrödinger suite. Here, the MDM2-p53 complex with Pdb_Id: 1YCR was used as an input and the grid computation done at the centre of the p53's transactivation domain. The outer grid box coordinates were set to 9.03, -14.57 and 24.22 in x, y and z axis respectively whilst the inner grid was kept at 10 angstroms (Å) for the same 3d axis. Both grids are very critical during docking as they give a true measure of the effective search space and enables all ligands to find usual and asymmetric binding modes within the active site whilst confining their midpoints into a smaller box to save calculation time. The van der Waals radius scaling was set to 1 to soften the potential for nonpolar parts of the receptor, and the partial charge was set to 0.25.

Virtual Screening and Receptor-based ligand docking

The entire database was screened and docked to the MDM2 p53 binding domain through a flexible docking protocol employing the Glide standard precision (SP) algorithm in Maestro. The nature of docking simulations employed by this algorithm are the same to that of the High Throughput Virtual Screening (HTVS), except that HTVS reduces the number of intermediate conformations throughout the docking funnel and the thoroughness of the final torsional refinement and sampling. During the docking process, the Mdm2 p53BD structure was kept rigid (not even the hydroxyl and thiol groups could rotate), and flexibility was induced to all docking ligands. This was achieved through expansion of each input structure by generating variations on the ionisation state, tautomer's, stereochemistry, and ring conformations. Ultimately, the binding energies or affinities of all poses were analysed to determine the best lead compounds.

Molecular dynamic simulations

To assess the binding specificity of the best lead compound - Ezetimibe, we subjected Ezetimibe-Mdm2 and nutlin-3a-Mdm2 complexes to molecular dynamics (MD) simulations. We used the Desmond module in Maestro v2021-2 with the OPLS4 force field. We restricted the complexes by an orthorhombic box on which the TIP3P water solvation model was utilized (Jorgensen et al., 1983). The volume of the box was minimized to centre the complexes, and sodium ions (Na^+) were added to counterbalance the overall charge on both systems. The Nose-Hoover thermostat[17] and Martyna-Tobias-Klein barostat[18] techniques were used to maintain the temperature and pressure at 300 Kelvin and 1.01325 bar, respectively. We executed the simulations with the NPT ensemble class, to ensure that the number of atoms, pressure, and timescales were kept constant. To simulate long-range electrostatic interactions, the Particle-Mesh-Ewald approach was used[17]. We also generated the RMSD and RMSF plots for Mdm2-Ezetimibe and Mdm2-Nutlin-3A complexes to understand the relative stability of the ligands in the receptor-binding pocket. Both simulations were monitored for 50 nanoseconds (ns), in which each had a 50 picosecond (ps) recording interval and generated 1000 frames. Finally, we used the MD trajectory analysis and simulation diagrams to analyze and present results.

In silico Pharmacokinetics.

ADMET (Absorption, Distribution, Metabolism and Toxicity) studies for Ezetimibe were conducted using SwissADME, ADMETSAR and ProTox II. We computed physicochemical properties such as molecular weight (MW), molecular refractivity (MR), the count of specific atomic types and Polar surface area (PSA) employing the TPSA (Topological polar surface area) fragmental technique (which considers sulfur and phosphorus as polar atoms), lipophilicity, water solubility, pharmacokinetics and drug-likeness.

Determination of cell viability by MTT Assay.

The cancer cell lines (A375, A549, HT-29, MCF7) and the normal cell line (HEK293) were plated in 96 well plates and grown till they reached a confluency of 80–90%. The cells were then treated with various concentrations of Ezetimibe for 48hrs in three biological replicates. Following treatment, 10 µl of the MTT reagent was added and cells incubated for a further 4 hours at 37°C. Dimethyl sulfoxide (DMSO) (D8418, Sigma Aldrich) was then added to the wells to solubilise the MTT crystals. The samples were incubated further for 15 minutes at 37°C and absorbance readings taken at 570 nM using the Varioskan™ LUX multimode microplate reader (ThermoFisher Scientific, VL0000D0) and Varioskan software. The percentage of cell viability was determined using the absorbance readings of treated and untreated cells using the formula below. The IC_{50} values for each cell line were calculated using the AAT Bioquest IC_{50} online calculator[19].

$$\%\mathrm{CellViability} = \frac{Absorbance\,(treated)}{Absorbance\,(untreated)} \times 100$$

Determination of cell cycle progression by flow cytometry.

The impact of Ezetimibe on cell cycle progression was determined using the propidium iodide staining method and flow cytometry analysis. Lung cancer (A549) and embryonic kidney (HEK293) cells were initially seeded in 6-well plates at a seeding density of 100,000 cells per well, each containing 2 ml of culture media. These cells were allowed to grow until they reached 80–90% confluency. Following this, the cells were treated with the IC50 concentration of Ezetimibe, with triplicate samples, and the treatment was sustained for 48 hours. Centrifugation (for floating cells) and trypsinization (for attached cells) were employed for cell collection. Subsequently, the cells were washed with 1X phosphate-buffered saline (PBS) twice to remove any residual culture media and other contaminants. The cells were then stained with propidium iodide (PI), a common DNA intercalating dye used to assess cell cycle status. The assessment of cell cycle alterations resulting from the Ezetimibe treatment was conducted using a BD FACS Aria III flow cytometer. This advanced analytical instrument enabled precise and detailed analysis of the cell populations, facilitating the determination of the impact of Ezetimibe on the cell cycle progression in the treated cells.

Immunocytochemistry.

Cells were cultured at 37°C, with 5% CO_2 in 89% DMEM, 10% FBS and 1% pen/strep media. Cells were seeded using trypsin-EDTA onto sterilised coverslips and grown until they reached a confluency of between 70 and 80%. The cells were fixed with 3% formaldehyde and permeabilised by 0.25% Triton X-100 in phosphate buffered saline (PBS) and blocked for 1 hour 30 minutes using 10% normal goat serum with 0.1% bovine serum albumin (BSA) before the primary antibody was added. The cells were then incubated at 4°C for 12–16 hours. After washing five times with PBS containing 0.1% Tween the cells were incubated in secondary antibody for one hour 30 minutes at 37°C in the dark and washed five times with PBS with 0.1% Tween. The procedure was repeated for the second set of antibodies for double-stained cells. A range of concentrations from 1:50 to 1:5000 of primary and secondary antibodies was used. Prolong Gold Anti-fade reagent with DAPI (Invitrogen) (10P36935) was used as mounting media and the nucleus stain. A Zeiss LSM 710 series confocal fluorescence microscope with Zen Black imaging software was used to analyse the stained cells. ImageJ software [20] with the JACoP plugin [21] was used to quantify colocalization analysis.

Coimmunoprecipitation.

Cells were sonicated on ice for five cycles of 10 seconds at 60 Amps. The lysed cells were then centrifuged at 12,100 x g for 20 minutes at 4°C before adding 50 µl/ml of protease inhibitor. After adding the primary antibody, the mixture was incubated for 5 hours at 4°C, with rotation. Next, Protein A agarose was added to the cell lysate/antibody mixture and incubated for another 12–16 hours at 4°C with rotation. Any unbound protein was removed, and the beads were washed five times with PBS and centrifuged at 1000xg for 5 minutes. Proteins were eluted off the beads by boiling the beads with SDS-PAGE sample buffer. Samples were then analysed using SDS-PAGE and Western blot.

Western blot.

Western blot analysis was conducted either according to Towbin et; al[22] or by using the automated system, Jess™ Automated Protein Immunodetection and Quantification (Biotechne). Protein samples were run on 10 %SDS-PAGE and then transferred onto PVDF membranes using transfer sandwiches. The transfer occurred overnight at 40 V at 4°C. Next, membranes were blocked with Sigma casein blocking buffer for 1 hour at room temperature. Next, membranes were incubated in primary antibody (1:10000 for RBBP6 and p53, 5:10000 for Mdm2) overnight at 4°C with shaking. Membranes were washed with TBST before being incubated in HRP conjugated secondary antibody (1:10000) for 1 hour 30 minutes at room temperature with shaking. Membranes were again washed with TBST before being stained with Chemiluminescent substrate (Thermo Scientific, Massachusetts, United States).

To determination of protein expression levels of cell cycle related proteins following treatment in A375, A549 and HEK293 cells was conducted test using the JessTM automated Western Blot system (ProteinSimple, Bio-techne) and the 12–230 kDa Separation Module (SM-W001, ProteinSimple). The, total protein was firstly extracted from treated and untreated cells using the Lytic M cell lysisCeLytic M reagent (C2978, Sigma Aldrich) Merck Millipore, Germany) mammalian cell lysis reagents. The protein samples

were denatured through heating for 10 minutes atminutes at 95°C. The protein concentrations were determined using the Qubit™ Protein Broad Range (BR) Assay Qubit Protein Assay (A50668, Thermo Fisher Scientific, United States) and measured by spectrophotometry using Qubit™ Flex Fluorometer Qubit Fluorometer (Thermo Fisher Scientific, United States). Ten microlitres of protein samples were mixed with 2 µL of master mix and incubated at 95°C for 5 minutes. Ten microlitres of protein samples were loaded on to a 25 well plate/module preloaded with buffers. Five microlitres of 1:50of 1:50 anti-RBBP6 (ab237514, abcam), and 1:50and 1:50 anti-p21 (ab109420, abcam) primary antibodies were added to detect the RBBP6, protein andand p21 proteins in a multiplex reaction. The 25 well chemiluminescence cartridge was used for the separation and immunodetection of proteins. The samples were run on the Jess automated immunodetection and quantification (ProteinSimple, Bio-techne) for 3 hours and data analysis done using the Compass software version 6.2.0 (ProteinSimple, Bio-techne).

Determination of cell cycle progression by flow cytometry.

The impact of Ezetimibe on cell cycle progression was determined using the propidium iodide staining method and flow cytometry analysis. Lung cancer (A549) and embryonic kidney (HEK293) cells were initially seeded in 6-well plates at a seeding density of 100,000 cells per well, each containing 2 ml of culture media. These cells were allowed to grow until they reached 80–90% confluency. Following this, the cells were treated with the IC_{50} concentration of Ezetimibe, with triplicate samples, and the treatment was sustained for a period of 48 hours. A combination of centrifugation (for floating cells) and trypsinization (for attached cells) was employed for cell collection. Subsequently, the cells were washed with 1X phosphate-buffered saline (PBS) twice to remove any residual culture media and other contaminants. The cells were then stained with propidium iodide (PI), a common DNA intercalating dye used to assess cell cycle status. The assessment of cell cycle alterations resulting from the Ezetimibe treatment was conducted using a BD FACS Aria III flow cytometer. This advanced analytical instrument enabled precise and detailed analysis of the cell populations, facilitating the determination of the impact of Ezetimibe on the cell cycle progression in the treated cells.

Statistical Analyses.

All statistical analyses were performed using Prism GraphPad Software (San Diego, CA 92108, USA). The cell viability data were expressed as the mean ± standard deviation (SD) from three independent experiments. The IC_{50} values for each cell line were calculated using the AAT Bioquest IC_{50} online calculator. The one sample T-test and Wilcoxon Signed Rank Test were used to determine the statistical difference between the cell viability percentage in treated cells. The *p* values less than 0.05 were regarded as statistically significant.

Results

Molecular docking of Ezetimibe and nutlin3a to the Mdm2-p53 binding domain

The molecular docking studies show that Ezetimibe binds to the same binding pocket of Mdm2 as the Nutlins. The chemical name for Ezetimibe is 1-(4- fluorophenyl)-3(R)-[3-(4-fluorophenyl)-3(S)-hydroxypropyl]-4(S)-(4-hydroxyphenyl)-2-azetidinone. It belongs to the azetidinone class of compounds which are characterized by a β-lactam ring and a grey surface representation of Ezetimibe and its superposition with p53 is shown in Fig. 1A and 1D.

Nutlins are spirooxindole compounds which were developed as non-peptidic mimics of the p53 peptide that binds to Mdm2. Based on our docking studies, Ezetimibe binds snuggly into the same binding site as nutlin3a, which is now in clinical trials for the treatment of cancer. Therefore, this study revealed Ezetimibe as a highly effective inhibitor upon targeting the Mdm2-p53 binding domain with a docking score of -7.919Kcal/mol (Table 1). Notably this binding energy was better than the − 6.359Kcal/mol observed in the case of nultin3a (Table 1).

Furthermore, the active site is also dominated by a mixture of highly hydrophobic and polar residues (Figs. 1 and 2), and both drugs make multiple hydrophobic and polar interactions to facilitate the binding coordination. Primarily three hydrophobic pockets in Mdm2 defined by critical side chains on the p53 peptide, namely, Phe19, Trp23, and Leu26 form the main anchor of the Mdm2-p53 Interaction [23].Moreover, a superimposition of Ezetimibe to the p53 peptide in the context of the Mdm2 binding site shows a good alignment indicating that Ezetimibe may be a better competitive inhibitor for p53 (Fig. 1C **and D**) than the nutlins.

Table 1
A comparison of the molecular and in *silico* ADME profiles of Ezetimibe and nutlin3a.

Properties	Ezetimibe	Nutlin-3a
IUPAC name	(3R,4S)-1-(4-fluorophenyl)-3-[(3S)-3-(4-fluorophenyl)-3-hydroxypropyl-4-(4-hydroxyphenyl) azetidin-2-one	4-(4,5-bis(4-chlorophenyl)-2-(2-isopropoxy-4-methoxyphenyl)-4,5-dihydro-1H-imidazole-1-carbonyl) piperazin-2-one
Estimated free energy of binding/docking score (Glide v2021-2)	-7.919 kcal/mol	-6.359 kcal/mol
Molecular weight	409,433g/mol	581,494 g/mol
Hydrogen bond acceptor	5	5
Hydrogen bond donor	2	1
Rotatable bonds	6	8
Rule of five (No. of violations)	1	4
ClogP	4.33	4.56
Solubility (SILICOS-IT)	$2.55x10^{-5}$mg/ml	$4.12x10^{-7}$mg/ml
Blood-brain barrier (ADMETSAR probability)	0.9074	0.7397
Human intestinal absorption (ADMETSAR probability)	0.9899	1.0000
Carcinogens (ADMETSAR probability)	0.8328	0.6361
Acute oral toxicity (ADMETSAR probability)	0.5892	0.6605
Aqueous solubility (logS) (ADMETSAR)	-3.8761	-3.2817
Rat acute toxicity (LD_{50}, mol/kg) (ADMETSAR)	2.4979	2.5907

Properties	Ezetimibe	Nutlin-3a
Solvent accessibility or polar surface area ($Å^2$)	60.77$Å^2$	83.47$Å^2$
Binding residues (Mdm2- p53BD)	VAL93, LYS94, GLN72, GLY58, PHE86, ILE103, LEU82, PHE91, LEU57, LEU54, ILE99, TYR100, TYR67, MET62, ILE61	VAL93, GLN72, GLY58, LEU54 ILE99, TYR100, MET62, ILE61

Importantly, Ezetimibe fits well in the three binding pockets in which the glucuronidation site is positioned to the Phe19 pocket whilst the hydrogen bond it forms with VAL93 is in the Trp23 pocket. This hydrogen bond that Ezetimibe forms is interesting because Trp23 in the p53 peptide also forms a hydrogen bond with this residue and this interaction has been reported to be crucial for p53-Mdm2 binding[24]. Additionally, Ezetimibe also forms a π–π stacking interaction with His96 which should augment the binding energy. The binding pocket induced by Ezetimibe is much smaller compared to the bulky nutlin3a-induced pocket. (Fig. 2). The topological arrangement described here would be sterically bulky for the glucuronidated version which binds to the Niemann-Pick C1-Like 1 receptor. Altogether these features suggest that only the parent drug would play the competitive role with p53.

Molecular Dynamic Analysis.

Molecular dynamics of Ezetimibe and nutlin3a in the Mdm2 hydrophobic pocket.

We conducted simulation studies on Ezetimibe binding to the Mdm2 hydrophobic pocket to understand the configurational adaptability during the molecular recognition process. For comparison, we performed the same simulations on nutlin3a bound to Mdm2. Throughout the simulation, the Mdm2-Ezetimibe interactions were observed for 50 ns. The RMSD for Ezetimibe depicts a consistent interaction pattern with the Cα atoms of the Mdm2 receptor **(**Fig. 3A **and B).** In contrast, the profile for nutlin3a suggests that it has little resident time in the binding pocket. It was observed that from approximately 15 to 47nsecs the nutlin3a drug candidate was completely not in contact with the Cα atoms of the Mdm2 protein (Fig. 3C). This is significant because it shows that nutlin3a was dissociated from the complex for 64% (32 nsecs) of the simulation period (Fig. 3). In contrast, there are persistent interactions between Ezetimibe and Mdm2 throughout the simulation period. Potentially, therefore, Ezetimibe could be a better antagonist to Mdm2-p53 interaction compared to nutlin3a. The RMSF data also depict an excellent trend in the case of Ezetimibe, with all interacting residues (indicated in green vertical lines) in their lowest energy state **(**Fig. 3B**)**. This occurs partially on the nutlin3a, because there is an N-terminal interacting residue exhibiting extreme fluctuations which may have caused the compromised thermodynamic stability of the Mdm2-nutlin3a complex (Fig. 3C **and D**). Notably, the RMSF data further reinforces that the Mdm2-Ezetimibe complex is more thermodynamically favourable than that of Mdm2-nutlin-3a.

Binding Interaction analysis

To analyse the thermodynamic profile of the Ezetimibe-Mdm2 Interaction within the Mdm2 pocket, we probed the binding coordination formed by Ezetimibe and compared it with that of nutlin3a. This analysis investigated four interactions—hydrogen bonding, hydrophobic interactions, ionic bonds, and salt bridges (Fig. 4). Both drugs showed no ionic bond interactions with the binding pocket. However, hydrogen bonds, hydrophobic and water bridge interactions facilitate the binding interactions in both complexes. Notably, Ezetimibe- interactions are dominated by hydrophobic forces and water bridges (Fig. 4A). Additionally, ILE61, GLN72, VAL93, HIS96, and ILE99 are the five most critical residues facilitating the binding coordination of the complex **(**Fig. 4B**)**.

Most importantly, the interaction fraction of Mdm2 is very low towards Nutlin3a (i.e., ≤ 0.5) compared to Ezetimibe (≤ ~ 0.98) as depicted in Figs. 4A and 5A. This further implies that Ezetimibe forms more stable complexes to the Mdm2-p53 binding domain, with an approximately up to 98% interaction fraction compared to the 50% observed in the case of nutlin3a (Figs. 4 and 5).

Nutlin-3A also showed that hydrophobic interactions and water bridges dominate the binding interactions it exhibits towards the Mdm2 receptor, and LEU54, PHE55, GLN59, ILE61, and VAL93 are the five critical residues facilitating the binding coordination (Fig. 5A **and B**). However, it is worth noting that the points of contact on the Mdm2-Nutlin3A complex are not persistent throughout the simulation as depicted in Fig. 5B. This observation further confirms that nutlin3a exhibits a lower drug resident time and may be frequently displaced during the simulation.

The pharmacokinetic properties of Ezetimibe and nutlin-3a

The *in silico* study of Ezetimibe pharmacokinetics was conducted as described in "methods' and the Ezetimibe profile was compared with nutlin3a (Table 1) to evaluate the drug-likeness of Ezetimibe. Ezetimibe has a single rule of five violation whereas nutlin3a has four. It has a lower molecular weight of 409,433 g/mol compared to nutlin3a (581,494g/mol). Furthermore, Ezetimibe and nutlin3a have comparable lipophilicity with cLogP values of 4.33 and 4.56 respectively. However, due to pre-systemic metabolism they have poor oral bioavailability.

A plausible therapeutic inhibitor of Mdm2, should have the following desirable properties: (a) a high binding affinity and specificity (b) potent cellular activity in cancer cells with wild-type p53, and (c) a highly desirable pharmacokinetic profile [25]. Ezetimibe has satisfactory properties and deserves an investigation as an anticancer agent.

Subcellular localization of RBBP6 and p53 in normal and cancer cell lines

There is extensive coverage of RBBP6 expression profiles in the Human Proteome Atlas. This resource shows that RBBP6 is prominently expressed in nuclear speckles in HEK293 cells, in several cancer lines and in different human tissues. Tissue distribution includes the brain, endocrine, respiratory, kidney, muscle, skin, proximal digestive, gastrointestinal, hepatic, the female and male reproductive tissues. These data show remarkable expression in lymphoid tissue and in myeloid cell lines. Furthermore, the

Human Protein Atlas data show that RBBP6 is involved in critical biological processes including, metabolism, DNA repair, signal transduction and the immune system. Finally, RBBP6 is shown to be overexpressed in many cancers including, gliomas, head and neck, lung, colorectal, prostate, breast, ovarian, cervical, melanoma, liver, and thyroid cancers.

Although RBBP6 is a negative regulator of p53 their subcellular Interaction has not been reported. Furthermore, the p53-Mdm2-RBBP6 Interaction has not been elucidated in human cells. Early studies show that p53 has nuclear and cytoplasmic functions, as a transcription factor in the nucleus and as cytoplasmic signaling molecule [26–30]. Recently, a review of p53's cytoplasmic functions was conducted [30]. In the current study, we find that p53 and RBBP6 have an inverse relationship in a normal cell line (HEK293 T) where RBBP6 is expressed, almost exclusively, in nuclear speckles while p53 is distributed throughout the cell but more prominently in the cytoplasm (Fig. 6). In contrast, RBBP6 is conspicuously detectable in the cytoplasm of the cancer line MCF7 in addition to nuclear speckles and p53 is expressed more prominently in the nuclei of the cancer cell lines compared to the normal cell line. In the A549 cell line RBBP6 and p53 have distinct inverse subcellular localization and concentration profiles. In MDA-MB-231 cells whose p53, is mutated in the DNA binding domain, both RBBP6 and p53 are more highly expressed in the cytoplasm than in the nucleus.

To determine if there was subcellular colocalization between p53 and RBBP6 we used an RBBP6 primary antibody that recognises isoforms 1, 2, and 4 based on the epitope specified by the manufacturer. This means this antibody cannot recognise isoform 3, the shortest isoform of RBBP6, known as DWNN. Isoform 3 has been found to be localised in the cytoplasm and to be pro-apoptotic [31]. Cells were dually stained with antibodies that recognise RBBP6 and p53 in MCF7 cells and A549 cells (Fig. 7). Quantitative analysis was undertaken on the colocalization images using ImageJ colocalization JACoP plugin software[21]. Manders and Pearson's coefficients were generated and are displayed in Table 2. Colocalization was calculated for RBBP6 to p53 as well as p53 to RBBP6. The background threshold was set using the Costes method[32] to prevent bias. Manders overlap coefficient measures the co-occurrence, and Pearson's correlation coefficient measures if there is a correlation. Colocalization analysis of the Pearson Coefficient (r) indicates that a portion of the two molecules colocalizes (r = 0.759). Alternatively, colocalized expression of RBBP6 and p53 is confined in discreet regions within the nucleus.

The measurements in Table 2 show positive colocalization occurring in both cell lines, with the Manders coefficient values indicating a higher colocalization of RBBP6 to p53 than p53 to RBBP6 in both MCF7 and A549 cells. The values do not indicate a perfect colocalization value of 1; however, this is expected as both p53 and RBBP6 are involved in several biological functions within the cell that do not relate to their Interaction. On basic visual inspection, p53 and RBBP6 do not colocalise in the nuclear speckles.

Table 2

Quantitative colocalisation measurements. *Manders and Pearson's coefficients were calculated using the JACoP plugin of ImageJ*[21] *for MCF7 and A549 cells.*

Measurement	MCF7	A549
Mean Manders coefficient of RBBP6 to p53	0.904	0.834
Mean Manders coefficient of p53 to RBBP6	0.761	0.784
Mean Pearson's coefficient	0.759	0.630

The RBBP6-p53-Mdm2 complex

Coimmunoprecipitation: Both Mdm2 and p53 are complexed with RBBP6.

We explored the potential p53/Mdm2/RBBP6 complex formation using coimmunoprecipitation on lysates of normal and cancer cell lines, HEK293T and MCF7, respectively. Briefly, the lysate was mixed with either an anti-p53 or anti-RBBP6 antibody, and complexes were pulled using Protein A. These complexes were visualized by Western blot analysis. Bands corresponding with p53, Mdm2, and RBBP6 were detected in complexes derived from the cancer and normal cells (Figs. 8 and 9). The Mdm2-p53-RBBP6 physical interaction is demonstrated by Western blot analysis.

Ezetimibe is a potential anticancer drug targeting the p53/Mdm2/RBBP6 complex.

Currently, Ezetimibe is given orally to treat cholesterolemia. It is activated in the intestines into the pharmacologically active Ezetimibe glucuronide. The results from the current study indicate that the parent drug binds to Mdm2, the prototypical negative regulator of p53. This study shows that Ezetimibe is toxic to specific cancer cell lines, such as A375 and A549. It is not toxic to a normal human embryonic kidney cell line at the same concentrations. Therefore, Ezetimibe may be a candidate for anticancer therapy when given parenterally to bypass pre-systemic metabolism.

Ezetimibe Toxicity to cancer cell lines.

We tested the toxicity of Ezetimibe to several human cancer lines, including the human melanoma cell line, A375, the human pancreatic cell line (PANC-1), the breast cancer cell line (MCF7), lung cancer cell line (A549), the colorectal cell line (HT-29) and the normal human embryonic kidney cell line (HEK293) using the MTT assay. Ezetimibe strongly inhibits the growth of the melanoma (A375) and lung cancer (A549) cell lines with IC_{50} concentrations of 30.7 µM and 48.34 µM respectively compared to the lung cancer cell line and the pancreatic cancer cell line (Fig. 10). At these concentrations Ezetimibe does not exhibit toxicity to the normal human embryonic kidney cell line (HEK293), breast cancer cells (MCF7) and the p53 negative colorectal cell line (HT-29). Interestingly, previous studies showed that Mdm2 and Mdm4 are highly expressed in melanoma[3334]. Ezetimibe inhibits approximately 20 % o the melanoma cell line at the lowest concentrations tested (1 µM) and more than 80 % a highest concentration (200 µM).

Notably, HT-29 cells are characterized by the overproduction of the p53 tumour antigen, harbouring a mutation at position 273 where arginine is replaced by histidine[35]. Studies have shown that this mutation in the *Tp53* gene significantly influences cancer cell responses to treatment. HT-29 cells, carrying the mutant p53, exhibit heightened resistance to the cytotoxic actions of certain drugs compared to cell lines with wild-type p53[35]. This resistance mechanism has also been observed in PANC-1 cells, which share the same mutation at position 273, notably affecting drug responses within the p53 pathway [36–38].

In the context of Ezetimibe treatment, it was observed that the mutant p53 in HT-29 and PANC-1 cells impacted their response differently compared to other cell lines tested. Despite the documented cytotoxicity of Ezetimibe in A549 and A375 cancer cell lines, PANC-1 displayed cell death at concentrations above 100 µM, while HT-29 cells showed no signs of cytotoxicity across all concentrations. This unique behavior emphasizes the complex interplay between Ezetimibe and the altered p53 pathway in HT-29 and PANC-1 cells.It appears that Ezetimibe causes an arrest of cells at the G1 phase of the cell cycle (Fig. 11).

Ezetimibe treatment downregulates the p53/p21/RBBP6 axis and induces G1 cell cycle arrest.

Our cell biological studies show that Ezetimibe causes a G1 cell cycle arrest and early apoptosis in lung (A549) cancer cell line (Fig. 11). To assess the molecular mechanism underpinning cancer cell death after Ezetimibe treatment, we applied the drug to the melanoma cell line, A375, and the lung cancercell line, A549, and compared this to untreated cells and a normal cell line, HEK293 (Fig. 12). The cancer cell lines express RBBP6 long isoforms, and p21, but Ezetimibe treatment downregulates all of them except for a 66 kDa protein that the anti-RBBP6 antibody recognizes. Unsurprisingly, untreated HEK293 cells express a relatively small amount of the p21 protein. This result suggests that Ezetimibe deactivates the p53/p21 pathway and RBBP6 activity. However, our molecular profiling does not elucidate the mechanism by which cell death occurs since the p53/p21 pathway appears to be deactivated.

It appears that the binding of the drug to the Mdm2 pocket may not result in a single outcome because when we knocked down Mdm2 using siRNA the effect of the Ezetimibe was slightly reduced in cancer cell lines. However, in the normal cell line the trend was more cell death when the drug was applied to Mdm2-downregulated cells (results not shown).

Discussion

Ezetimibe possesses properties that make it a plausible anticancer therapeutic drug targeting the p53/Mdm2/RBBP6 complex when given parenterally. When administered orally, it is a cholesterol absorption inhibitor that blocks the intestinal absorption of dietary and biliary cholesterol and Ezetimibe monotherapy is recommended for the treatment of primary (heterozygous-familial or non-familial) hypercholesterolaemia in adults in whom initial statin therapy is contraindicated, but it is co-administered with statins under certain conditions[39]. Although Ezetimibe is successful for the treatment of cardiovascular diseases, there are anecdotal reports suggesting an anticancer therapeutic effect.

However, the proposed mechanism underpinning the reported anticancer effect is presumed to be the reduction of cholesterol. In the current study we report that Ezetimibe interferes with Mdm2/p53 binding. Mdm2 is the prototypical negative regulator of the tumor suppressor protein p53. We provide evidence that the anticancer activities are based on its binding to Mdm2. Ezetimibe anticancer activities have been proposed based on its reduction of cholesterol. This is the first report that shows a direct anticancer activity. We show that p53 and its negative regulators Mdm2 and RBBP6 can form a complex, implying that targeting RBBP6 can also have an impact on treatment strategies. Alternatively, agents that inhibit RBBP6 could be combined with Mdm2 inhibitors as anticancer treatment.

We characterized the relationship p53 has with its two negative regulators Mdm2 and RBBP6. The implication this relationship has for drug discovery and development is exemplified by Ezetimibe and suggests that combined inhibition of Mdm2 and RBBP6 might be a good anticancer strategy. We present evidence that shows that p53 and its two negative regulators, Mdm2 and RBBP6 probably form a complex at certain subcellular locations. However, there are spatio-temporal differences in subcellular localizations. There are two interesting observations with respect to subcellular locations of the two molecules. Firstly, in the normal cell line, RBBP6 is expressed most prominently in nuclear speckles, while p53 is prominent in the cytoplasm. This suggests that these two proteins have distinct functions in normal cells. The localization of RBBP6 in the nuclear speckles is consistent with its known function in pre-mRNA splicing [40–42]. It also suggests that such functions are independent of p53. According to our observations, p53 and RPBP6 colocalize at distinct subcellular sites and not in nuclear speckles. Secondly, in the cancer cell line A549, RBBP6 accumulates in the cytoplasm and p53 in the nucleus, but our calculations indicate some colocalization. This spatial switch is interesting because a regulatory relationship between the two molecules at the transcriptional level has not been reported so far.

We have demonstrated the possible formation of a Mdm2-p53-RBBP6 complex by Western blot analysis (Figs. 8 and 9). This is consistent with the observation in the mouse where RBBP6 is reported to enhance the activity of Mdm2 [12]. It is noteworthy that only the long isoforms of RBBP6 are revealed in this complex since the antibodies used do not recognize the DWNN module which has been shown to inhibit the function of the longer isoforms during RNA processing [43]

The evidence presented here suggests that Ezetimibe may be an effective anticancer drug when administered parenterally. Currently, Ezetimibe is administered as a prodrug which is activated in the brush border into an active Ezetimibe glucuronide. Our data show that Ezetimibe binds into the Mdm2-p53-binding domain remarkably mimicking the p53 N-terminal peptide. While Ezetimibe does not structurally resemble nutlins, based on molecular docking simulations Ezetimibe accurately mimics p53 binding to the Mdm2 hydrophobic cleft. Ezetimibe, however, has structural vulnerabilities that hinder its use as an anticancer agent, such as its conversion by metabolic enzymes in the intestines. This results in negligible bioavailability of Ezetimibe in the intestines and as such it is unsuitable for use in the treatment of colorectal cancers.

Conclusion

The current evidence indicates that Ezetimibe, in its parent form, may be used as an anticancer drug, The mechanism of action is like that of nutlins and should involve the reactivation of p53. Given its vulnerability to pre-systemic metabolism Ezetimibe would be given parenterally. To protect it from presystemic metabolism, the parent drug must be modified. We have confirmed the existence of the p53/Mdm2/RBBP6 axis. We suggest that a combined targeting of Mdm2 and RBBP6 could result is a potent anticancer drug approach.

Declarations

Availability of data and materials

All data generated or analysed during this study are included in this published article.

Funding

MN and BR are funded by Buboo (Pty) Ltd. SM is funded by the Department of Higher Education (South Africa). SM and SS are funded by the National Research Foundation (South Africa).

Authors' contributions

MN conceptualised and directed all the research activities. CT performed the computational biology simulations, analyses and data interpretation. BR, SM, CM and SS conducted the cell biology experiments, interpretation and data analysis. All authors wrote the manuscript.

Acknowledgements

All computational simulations were run using a Schrödinger suite in the LENGAU cluster hosted by the Centre for High Performance Computing (CHPC) and the National Institute for Theoretical and Computational Sciences (NITheCS) in Cape Town, South Africa.

References

1. Altmann, S. W. *et al.* Niemann-Pick C1 Like 1 Protein Is Critical for Intestinal Cholesterol Absorption. *Science (1979)* **303**, 1201–1204 (2004).
2. Garcia-Calvo, M. *et al.* The target of ezetimibe is Niemann-Pick C1-Like 1 (NPC1L1). *Proceedings of the National Academy of Sciences* **102**, 8132–8137 (2005).
3. Gu, J. *et al.* Ezetimibe and Cancer: Is There a Connection? *Front Pharmacol* **13**, (2022).
4. He, J. *et al.* NPC1L1 knockout protects against colitis-associated tumorigenesis in mice. *BMC Cancer* **15**, 189 (2015).
5. Nicolle, R. *et al.* Pancreatic Adenocarcinoma Therapeutic Targets Revealed by Tumor-Stroma Cross-Talk Analyses in Patient-Derived Xenografts. *Cell Rep* **21**, 2458–2470 (2017).

6. Solomon, K. R. *et al.* Ezetimibe Is an Inhibitor of Tumor Angiogenesis. *Am J Pathol* **174**, 1017–1026 (2009).
7. Zheng, Y. *et al.* Promotion of colorectal cancer cell death by ezetimibe via mTOR signaling-dependent mitochondrial dysfunction. *Front Pharmacol* **14**, (2023).
8. He, Q. *et al.* Ezetimibe inhibits triple-negative breast cancer proliferation and promotes cell cycle arrest by targeting the PDGFR/AKT pathway. *Heliyon* **9**, e21343 (2023).
9. Zilfou, J. T. & Lowe, S. W. Tumor Suppressive Functions of p53. *Cold Spring Harb Perspect Biol* **1**, a001883–a001883 (2009).
10. Zhang, Q., Zeng, S. X. & Lu, H. Targeting p53-MDM2-MDMX Loop for Cancer Therapy. in 281–319 (2014). doi:10.1007/978-94-017-9211-0_16.
11. Charmy Twala. DRUGS TARGETING THE RETINOBLASTOMA BINDING PROTEIN 6 (RBBP6). (University of the Witwatersrand, Johannesburg, 2017).
12. Li, L. *et al.* PACT is a negative regulator of p53 and essential for cell growth and embryonic development. *Proceedings of the National Academy of Sciences* **104**, 7951–7956 (2007).
13. Xiao, C. *et al.* RBBP6, a RING finger-domain E3 ubiquitin ligase, induces epithelial–mesenchymal transition and promotes metastasis of colorectal cancer. *Cell Death Dis* **10**, 833 (2019).
14. Wang, Q., Wei, S. & Xiao, H. RBBP6 induces non-small cell lung cancer cell proliferation and high expression is associated with poor prognosis. *Oncol Lett* (2020) doi:10.3892/ol.2020.11403.
15. Chi, S.-W. *et al.* Structural Details on mdm2-p53 Interaction. *Journal of Biological Chemistry* **280**, 38795–38802 (2005).
16. Zhao, Y., Bernard, D. & Wang, S. Small Molecule Inhibitors of MDM2-p53 and MDMX-p53 Interactions as New Cancer Therapeutics. *Biodiscovery* 4 (2013) doi:10.7750/BioDiscovery.2013.8.4.
17. Evans, D. J. & Holian, B. L. The Nose–Hoover thermostat. *J Chem Phys* **83**, 4069–4074 (1985).
18. Martyna, G. J., Tobias, D. J. & Klein, M. L. Constant pressure molecular dynamics algorithms. *J Chem Phys* **101**, 4177–4189 (1994).
19. AAT Bioquest, Inc. ,. Quest Graph™ IC50 Calculator. (2023).
20. Schneider, C. A., Rasband, W. S. & Eliceiri, K. W. NIH Image to ImageJ: 25 years of image analysis. *Nat Methods* **9**, 671–675 (2012).
21. BOLTE, S. & CORDELIÈRES, F. P. A guided tour into subcellular colocalization analysis in light microscopy. *J Microsc* **224**, 213–232 (2006).
22. Towbin, H., Staehelin, T. & Gordon, J. Electrophoretic transfer of proteins from polyacrylamide gels to nitrocellulose sheets: procedure and some applications. *Proceedings of the National Academy of Sciences* **76**, 4350–4354 (1979).
23. Vassilev, L. T. *et al.* In Vivo Activation of the p53 Pathway by Small-Molecule Antagonists of MDM2. *Science (1979)* **303**, 844–848 (2004).
24. Zhao, Y., Aguilar, A., Bernard, D. & Wang, S. Small-Molecule Inhibitors of the MDM2–p53 Protein–Protein Interaction (MDM2 Inhibitors) in Clinical Trials for Cancer Treatment. *J Med Chem* **58**, 1038–

1052 (2015).

25. Shangary, S. & Wang, S. Small-Molecule Inhibitors of the MDM2-p53 Protein-Protein Interaction to Reactivate p53 Function: A Novel Approach for Cancer Therapy. *Annu Rev Pharmacol Toxicol* **49**, 223–241 (2009).
26. Finlay, C. A., Hinds, P. W. & Levine, A. J. The p53 proto-oncogene can act as a suppressor of transformation. *Cell* **57**, 1083–1093 (1989).
27. Levine, A. J. p53, the Cellular Gatekeeper for Growth and Division. *Cell* **88**, 323–331 (1997).
28. Lane, D. P. p53, guardian of the genome. *Nature* **358**, 15–16 (1992).
29. Finlay, C. A., Hinds, P. W. & Levine, A. J. The p53 proto-oncogene can act as a suppressor of transformation. *Cell* **57**, 1083–1093 (1989).
30. Kroemer, G., Bravo-San Pedro, J. M. & Galluzzi, L. Novel function of cytoplasmic p53 at the interface between mitochondria and the endoplasmic reticulum. *Cell Death Dis* **6**, e1698–e1698 (2015).
31. Mbita, Z. *et al.* De-regulation of the RBBP6 isoform 3/DWNN in human cancers. *Mol Cell Biochem* **362**, 249–262 (2012).
32. Costes, S. V. *et al.* Automatic and Quantitative Measurement of Protein-Protein Colocalization in Live Cells. *Biophys J* **86**, 3993–4003 (2004).
33. Muthusamy, V. *et al.* Amplification of CDK4 and MDM2 in malignant melanoma. *Genes Chromosomes Cancer* **45**, 447–454 (2006).
34. Gembarska, A. *et al.* MDM4 is a key therapeutic target in cutaneous melanoma. *Nat Med* **18**, 1239–1247 (2012).
35. Ravizza, R., Gariboldi, M. B., Passarelli, L. & Monti, E. Role of the p53/p21 system in the response of human colon carcinoma cells to doxorubicin. *BMC Cancer* **4**, (2004).
36. Sun, C. *et al.* Characterization of the mutations of the K-ras, p53, p16, and SMAD4 genes in 15 human pancreatic cancer cell lines. *Oncol Rep* **8**, (2001).
37. Moore, P. S. *et al.* Genetic profile of 22 pancreatic carcinoma cell lines. *Virchows Archiv* **439**, (2001).
38. Deer, E. L. *et al.* Phenotype and genotype of pancreatic cancer cell lines. *Pancreas* vol. 39 Preprint at https://doi.org/10.1097/MPA.0b013e3181c15963 (2010).
39. National Insitute for Health and Care Excellence.
40. Boreikaite, V., Elliott, T. S., Chin, J. W. & Passmore, L. A. RBBP6 activates the pre-mRNA 3' end processing machinery in humans. *Genes Dev* **36**, 210–224 (2022).
41. Gao, S., Witte, M. M. & Scott, R. E. P2P-R protein localizes to the nucleolus of interphase cells and the periphery of chromosomes in mitotic cells which show maximum P2P-R immunoreactivity. *J Cell Physiol* **191**, 145–154 (2002).
42. Li, B. & Zhuang, W. Splicing Factor SRSF1 Promotes Tumorigenesis Via Oncogenic Splice-Switching and Predicts Poor Prognosis in Multiple Myeloma. *Blood* **138**, 1133–1133 (2021).
43. Di Giammartino, D. C. *et al.* RBBP6 isoforms regulate the human polyadenylation machinery and modulate expression of mRNAs with AU-rich 3' UTRs. *Genes Dev* **28**, 2248–2260 (2014).

Figures

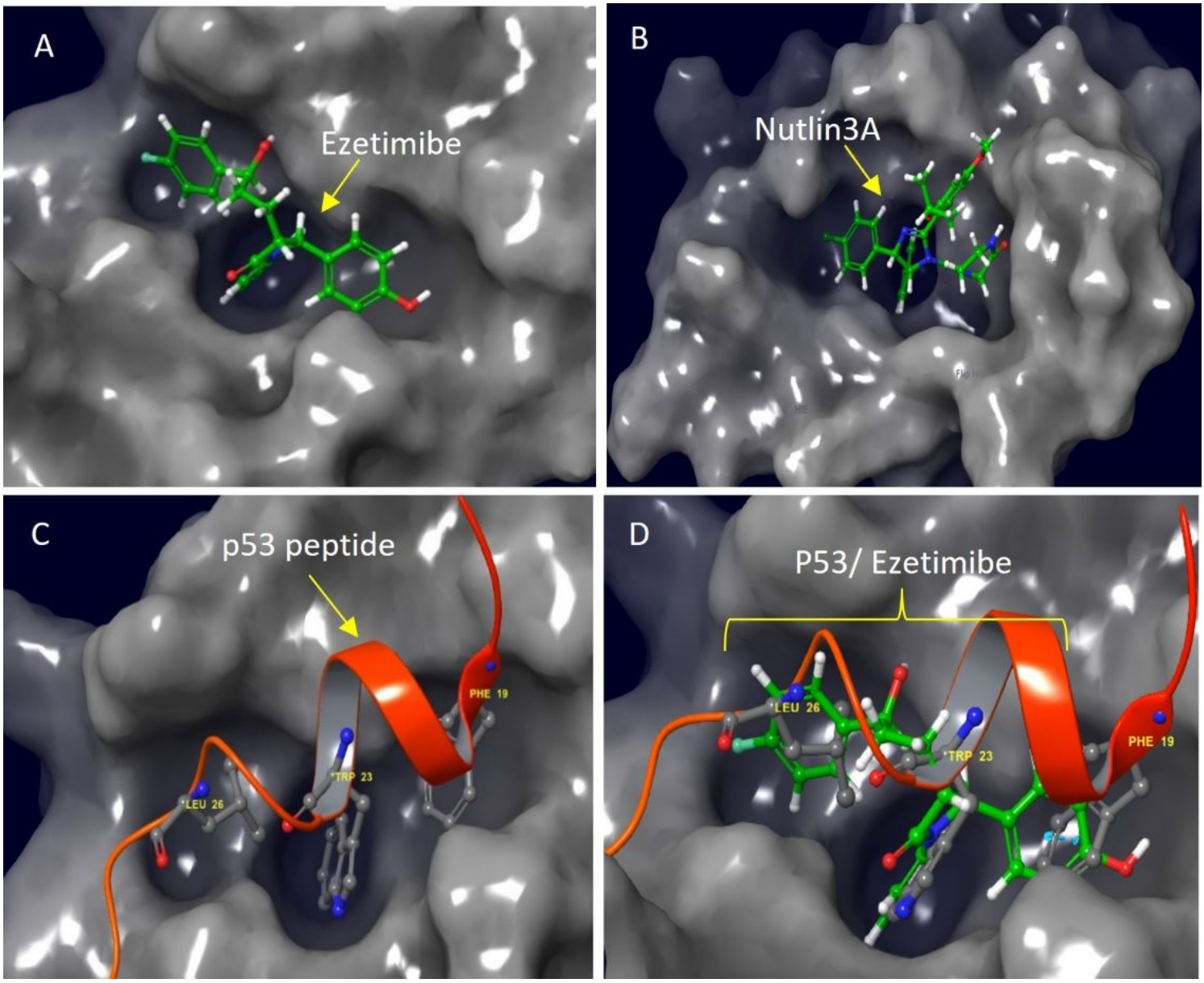

Figure 1

Molecular docking studies showing the most potent inhibitor of the Mdm2-p53 complex compared to Nutlin-3A. ***(A)*** *Shows the Ezetimibe molecule (green) bound into the Mdm2 hydrophobic cleft (grey surface),* ***(B)*** *indicates the Nutlin-3A drug docked into the same MDM2 pocket whilst,* ***(C)*** *Shows the p53 transactivation domain (red) also bound to the Mdm2 pocket (grey surface), the three critical residues (Leu26, Trp23 and Phe19) are also indicated in ball and stick models,* ***(D)*** *shows a graphical view of the Ezetimibe's inhibition activity, and the accurate mode of binding that mimics p53 upon targeting the Mdm2's hydrophobic cleft.*

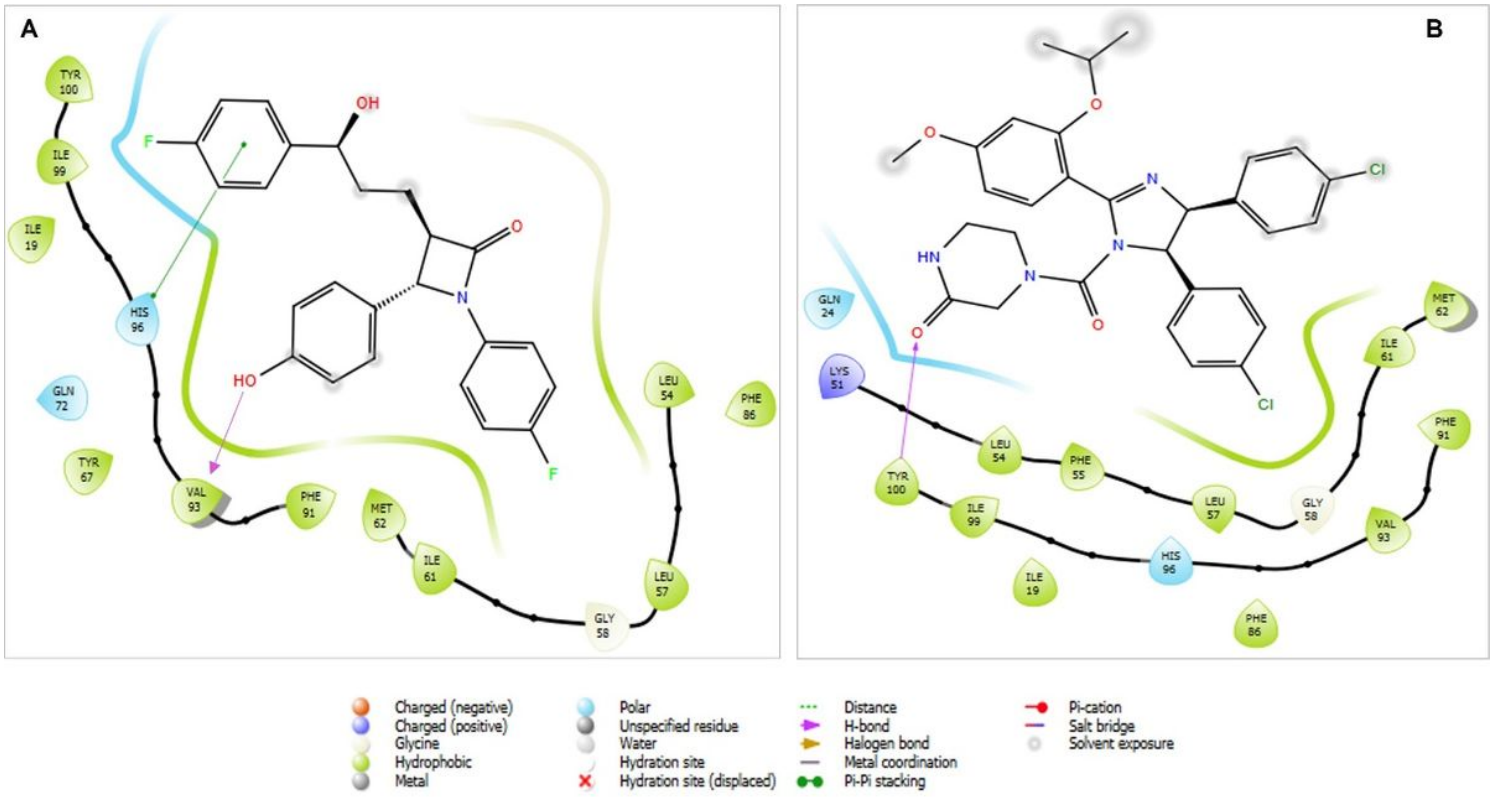

Figure 2

Two-dimensional ligand interaction diagrams of Ezetimibe and nutlin3a upon the Mdm2-p53 binding domain, (A) *indicates a 2D Interaction of MDM2-Ezetimibe complex in which the hydrophobic and polar residues dominate the binding coordination.* ***B****) Represents a 2D Interaction of MDM2-Nutlin3A complex in which the hydrophobic, polar and a single positively charged residue dominate the binding coordination. Note: Both diagrams were taken at 4Å axis around the compounds within the active site.*

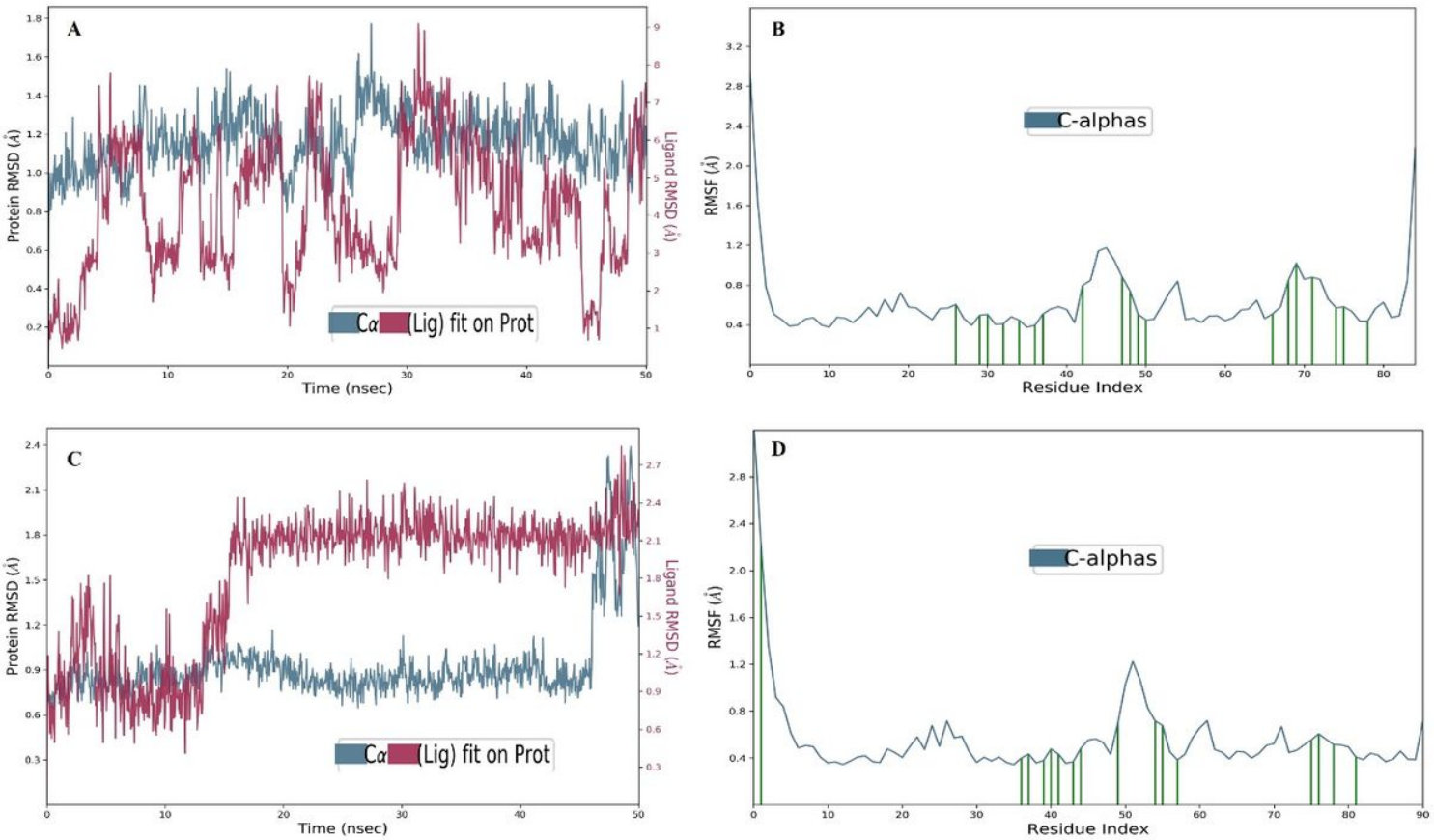

Figure 3

Molecular dynamic studies of Mdm2 complexed with Ezetimibe and nutlin3a (A) *Scalar distance of the Mdm2-Ezetimibe complex over a 50ns simulation time (The P-L RMSD); and* ***(B)*** *Characterization of the local protein fluctuation (The P_RMSF), with Ezetimibe interacting residues shown as green vertical lines.* ***(C)*** *Scalar distance of the MDM2-Nutlin3A complex over a 50ns simulation time (The P-L RMSD); and* ***(D)*** *Characterization of the local fluctuation of the protein (The P_RMSF), with nutlin3a interacting residues shown as green vertical lines. Note: RMSD stands for Root Mean Square Deviation, RMSF stands for Root Mean Square Fluctuation.*

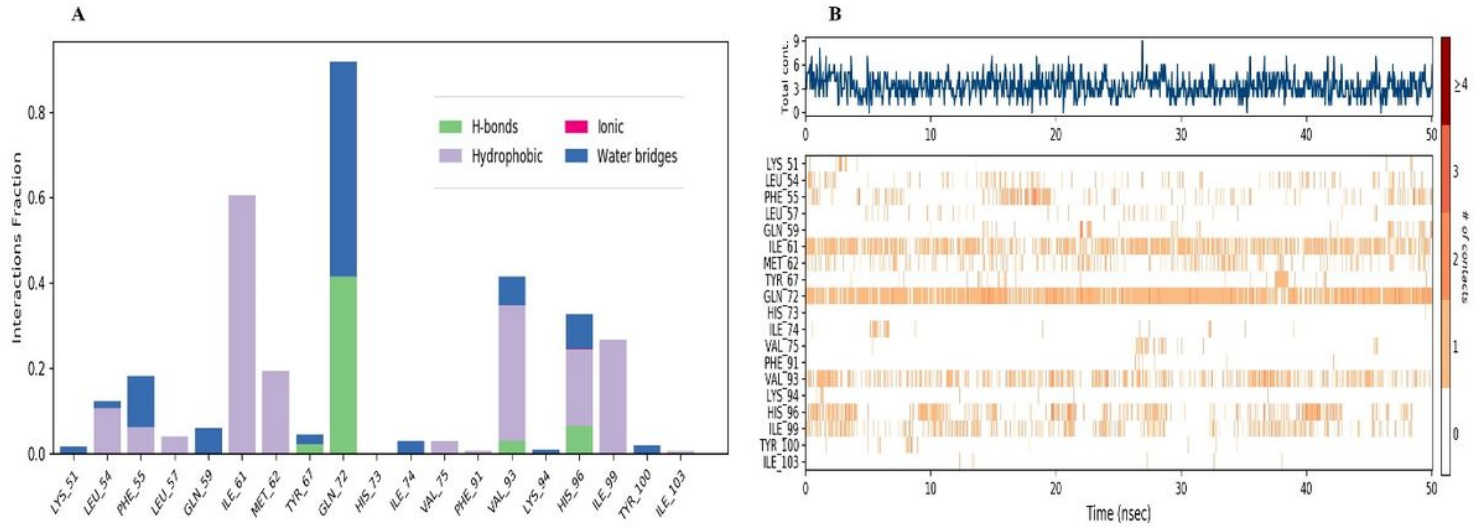

Figure 4

Protein-Ligand contacts of the Mdm2-Ezetimibe complex, (A) *Depicts the Interaction fraction per residue of the MDM2-Ezetimibe complex in which the hydrophobic and water bridge interactions dominate the binding coordination.* ***B****) Represents the extent of binding as well as the number of contacts made throughout the simulation.*

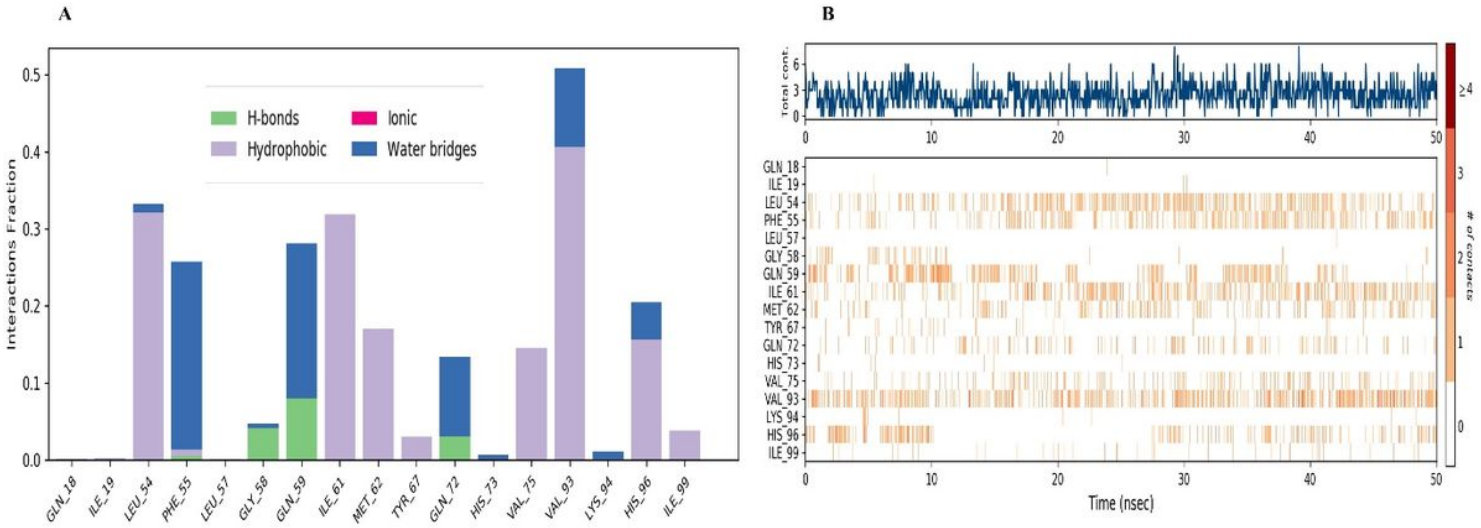

Figure 5

Protein-Ligand contacts of the Mdm2-nutlin3a complex. (A) *Interaction of Mdm2-nutlin3a complex in which the hydrophobic and water bridge interactions dominate the binding coordination.* ***B****) Represents the extent of binding as well as the number of contactsmade throughout the simulation.*

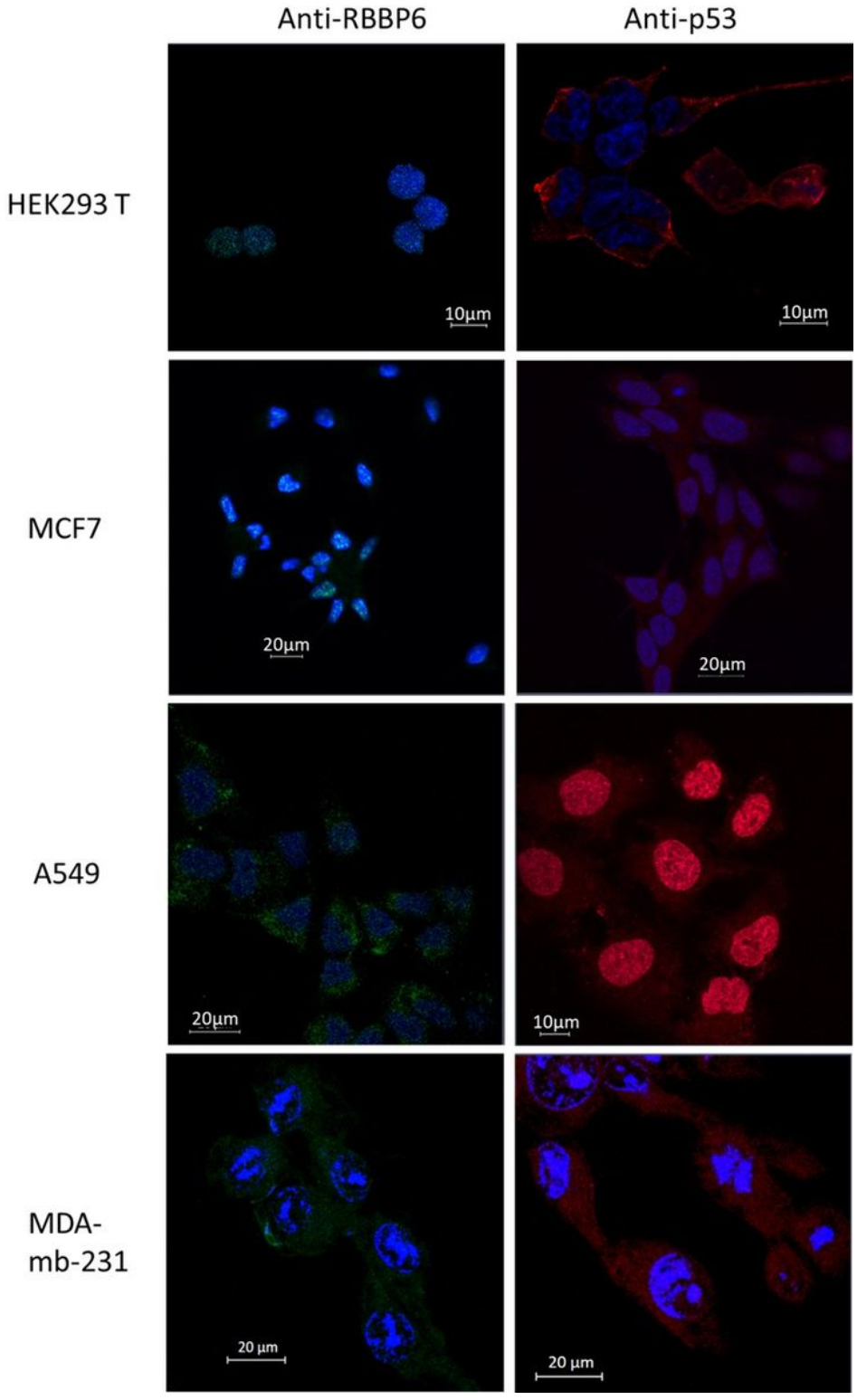

Figure 6

Localisation of RBBP6 and p53 in several cell lines. *HEK293 T, MCF7, A549 and MDA-mb-231 cell lines were stained with polyclonal anti-RBBP6 (green) and monoclonal anti-p53 (red). DAPI (blue) shows the stained cell nucleus. The scale bar is indicated for each cell line. Images were captured by confocal microscopy, using optimised gain and laser power settings as determined by controls.*

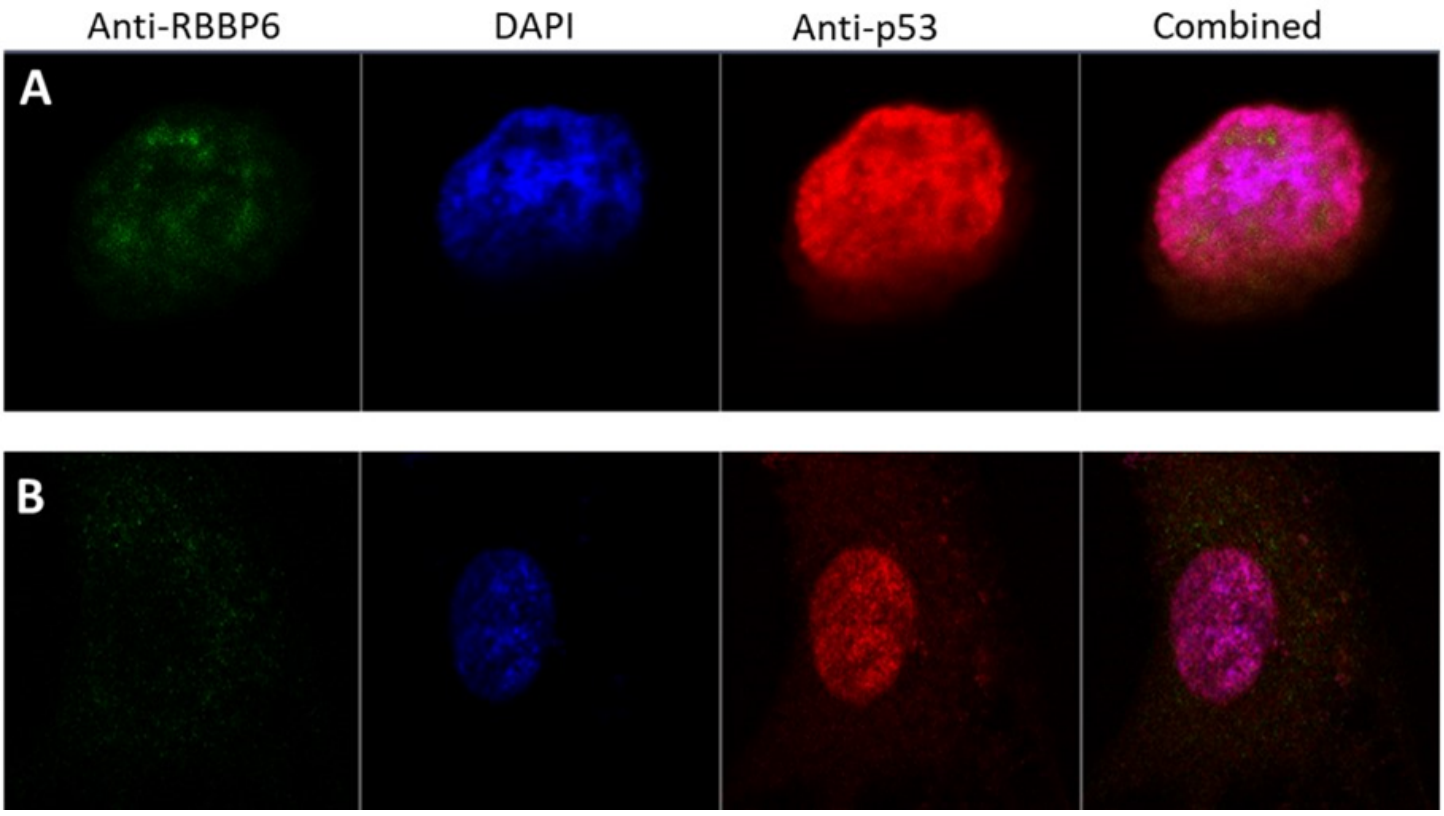

Figure 7

Colocalisation of p53 and RBBP6 in MCF7 cells and A549 cells. (A) *MCF7 cells were stained with polyclonal anti-RBBP6 (green) and monoclonal anti-p53 (red). The scale bar is 5μm.* ***(B)*** *A549 cells were stained with polyclonal anti-RBBP6 (green) and monoclonal anti-p53 (red). The scale bar is 10μm. DAPI (blue) shows the stained cell nucleus.*

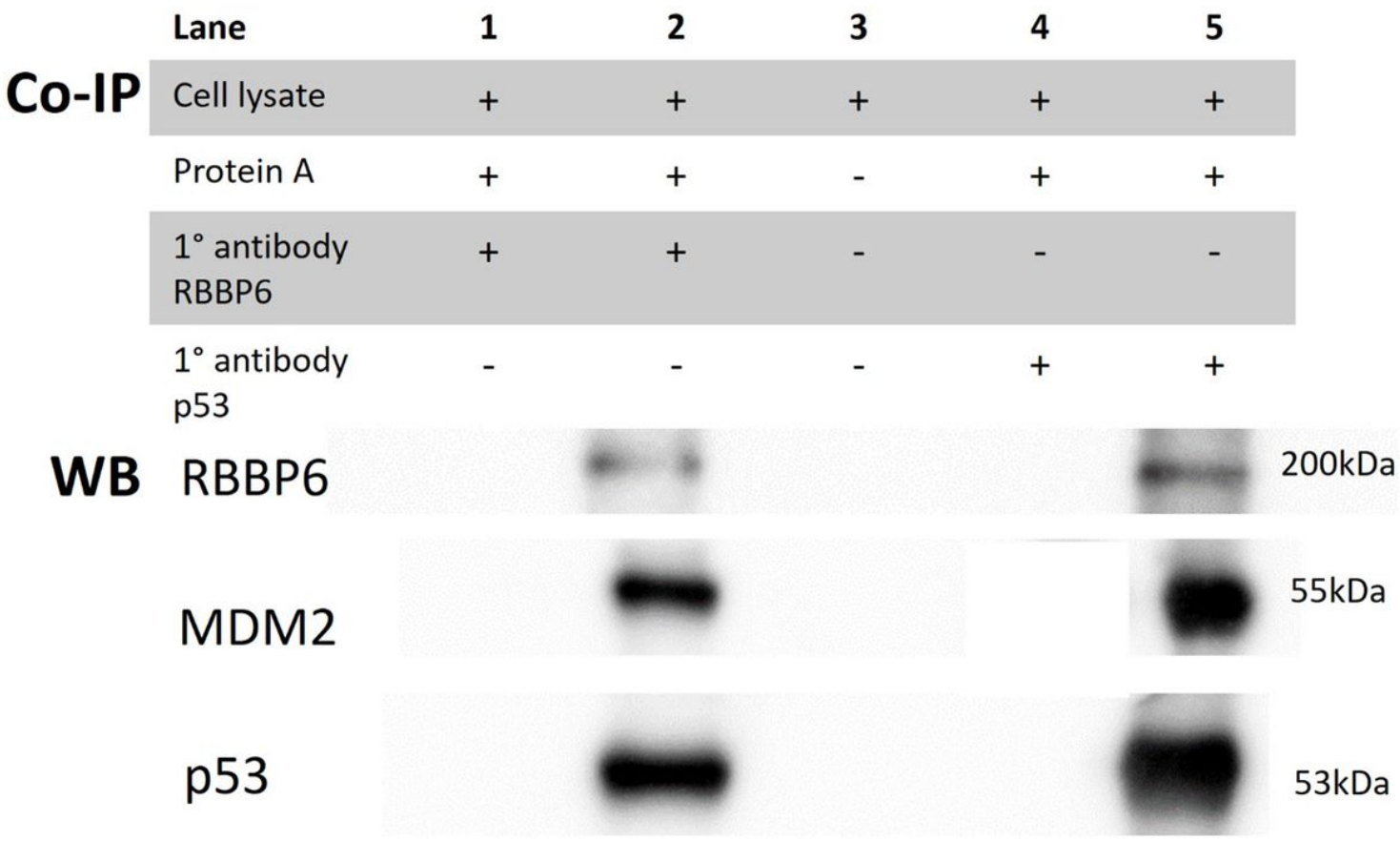

Figure 8

Western blot analysis on samples collected from Co-IP assays performed using RBBP6 and p53 antibodies on HEK293 T cells. *Three independent Western blots were performed to investigate the presence of p53, RBBP6, and MDM2 in Co- IP assays performed using crude cell lysate, Protein agarose A and anti-RBBP6 (lanes 1 and 2) and anti- p53 (lanes 4 and 5) respectively. Lanes 1 and 4 show the flow-through samples which contain the proteins in the crude cell lysate that did not interact with the Protein A agarose bound antibody. Lanes 2 and 5 contains the immuno-complexes isolated during the Co-IP assays. Lane 3 is the HEK293 T crude cell lysate used in Co-IP assays.*

Figure 9

Western blot analysis on samples collected from Co-IP assays performed using p53, MDM2, and RBBP6 antibodies on MCF7 cells. *Three independent Western blots were performed to investigate the presence of p53, RBBP6, and MDM2 in Co-IP assays performed using cruse cell lysate, Protein A agarose and anti-p53 (lanes 1 and 2), anti-MDM2 (lanes 3 and 4), and anti-RBBP6 (lanes 5 and 6) antibodies respectively. Lanes 1, 3 and 5 show the flow-through samples which contain the proteins in the crude cell lysate that did not interact with the Protein A agarose bound antibody. Lanes 2, 4 and 6 contain the immuno-complexes isolated during each Co-IP assay respectively.*

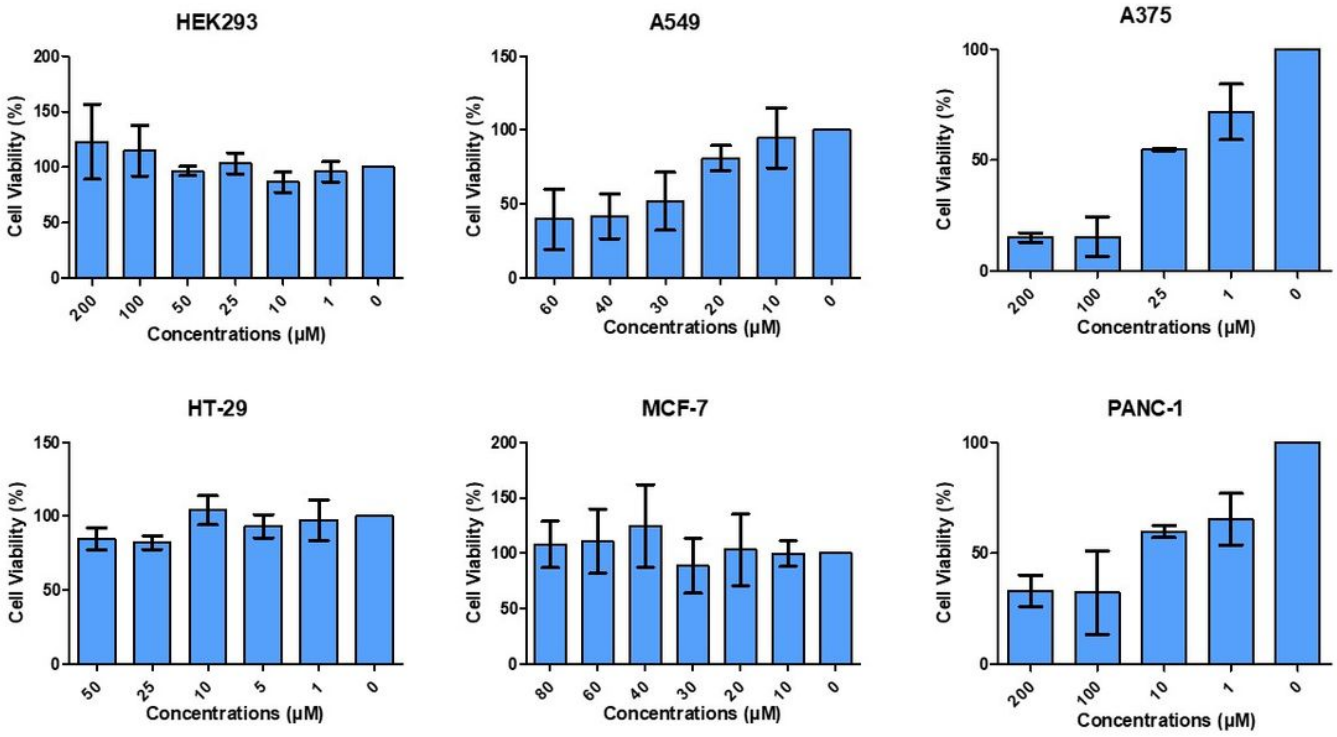

Figure 10

Cell viability MTT assay results showing treatment of various cell lines (HEK293, A549, A375, HT-29, MCF-7 and PANC-1) with Ezetimibe*. Whilst Ezetimibe is non-toxic to normal HEK293 cell line, concentrations above 30 µM are toxic to lung (A549) and melanoma (A375) cancer cell lines. IC50 values of 48.34 µM and 30.71 µM respectively Interestingly, Ezetimibe was found to be non-toxic towards breast (MCF7) and colorectal (HT-29) cancer cell lines.*

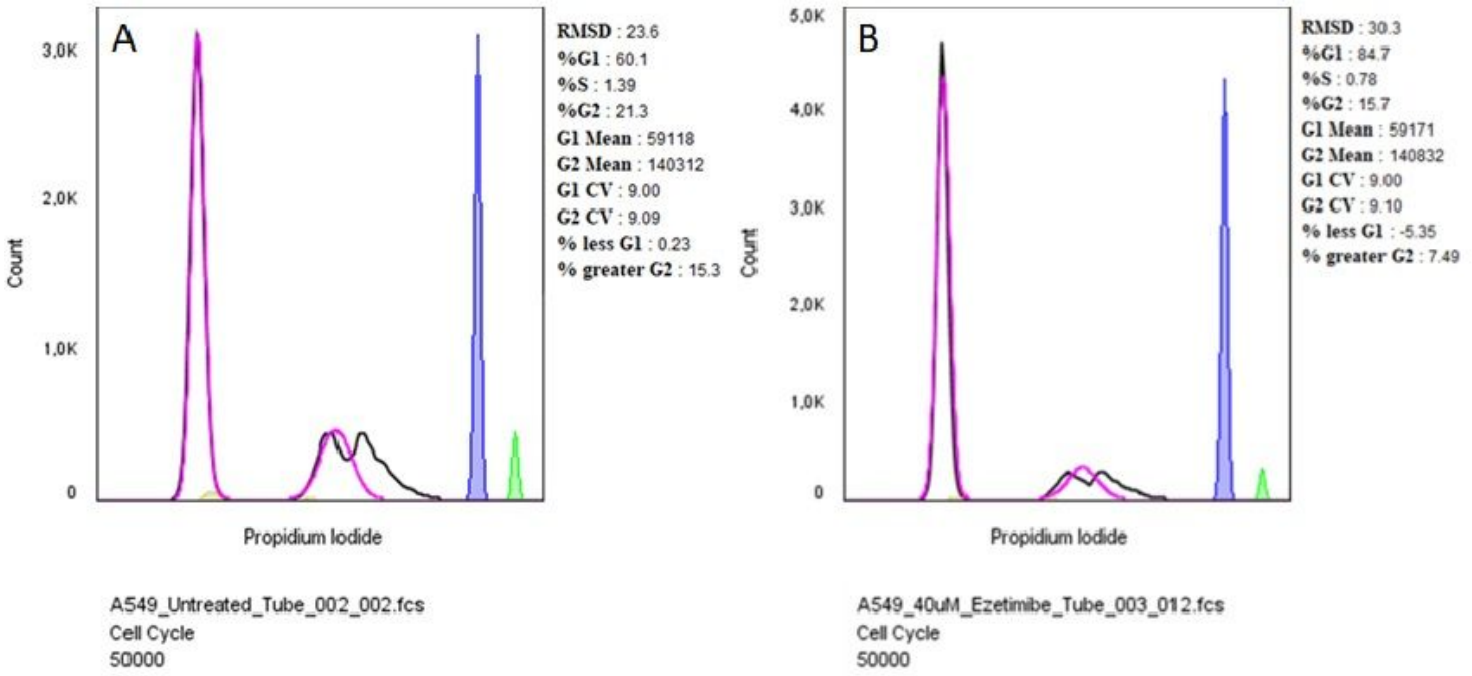

Figure 11

Cell cycle analysis of human lung adenocarcinoma (A549) cells treated with Ezetimibe*. Cells were stained with propidium iodide and analysed using the BD FACS Aria III.* ***(A)*** *Represents untreated A549 cells with 60 % of the cells in the G1 phase and approximately 36 % in the G2/M phase.* ***(B)*** *Represent A549 cells treated with 40 µM Ezetimibe. A 20 % increase in the number of cells in the G1 phase observed in treated cells compared to the untreated.*

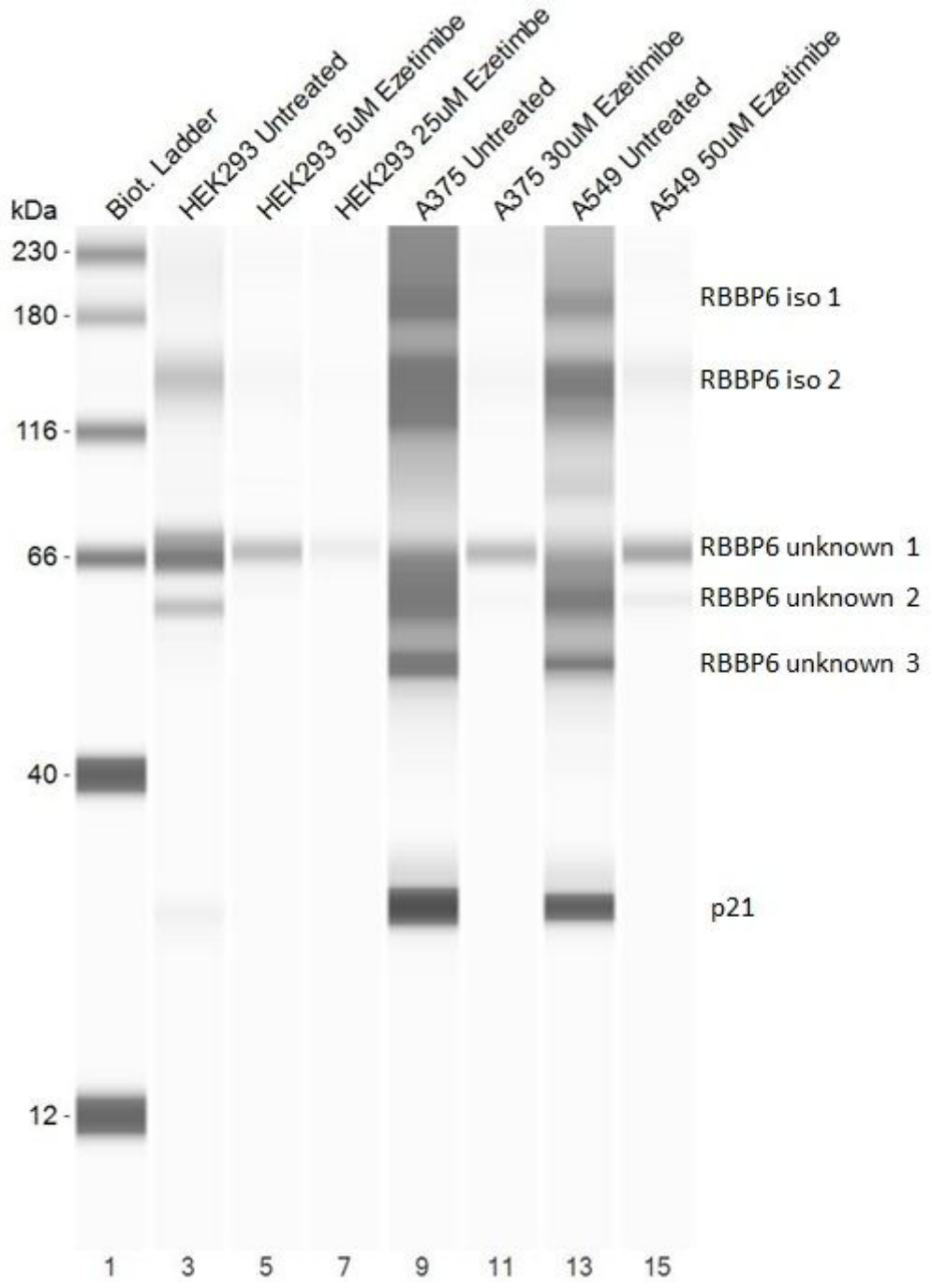

Figure 12

Image showing the immunodetection of RBBP6 and p21 in untreated and Ezetimibe treated HEK293, A375 and A549 cell lines*. The RBBP6 primary antibody cross reaction resulted in the detection of RBBP6 isoforms of known RBBP6 sizes and unknown sizes. The isoforms 1 ~200 KDa and isoform 2 ~ 116 kDa were detected in all untreated cell lines. There are three unknown bands (approx. 66 KDa, 55 kDa and 45 KDa) that were detected by the same antibody designated unknown 1, 2 and 3 respectively. All known and unknown isoforms are detected in untreated A549 and A375 cell lines whilst the treated cells exclusively express the 66 KDa unknown RBBP6 protein. The p21 protein is detectable in untreated A549 and A375 cells whilst almost absent in HEK293 (normal cells) and treated cancer (A549 and A375) cells. There is a clear difference between treated and untreated cell lines that requires further investigation.*

Supplementary Files

This is a list of supplementary files associated with this preprint. Click to download.

- Supplementaryfile1.Fullimagesofblots.docx